Supporting Information

Facile method to activate substrate for oxygen evolution by galvanic cell reaction

1. Experimental section

1.1 Chemicals

All reagents were of analytical grade and used without further purification. Ni foam (labeled as NF) and Fe foam (labeled as FF) were purchased from Suzhou Longshengbao Co., Ltd. Sodium chloride (NaCl), sodium fluoride (NaF), sodium bromide (NaBr), and sodium iodide (NaI) were purchased from Sigma-Aldrich. Potassium hydroxide (KOH) was purchased from Shanghai Meryer Chemical Technology Co. Ltd. Hydrochloric acid, ethanol, and acetone were purchased from Beijing Chemical Works. Milli-Q deionized water (resistance of 18.2 MΩ cm at 25 °C) was used for all experiments.

1.2 Synthesis Methods

1.2.1. Synthesis of GC NiFe LDH

In a typical experiment, NF and FF (10×40 mm, 1 mm in thickness) were ultrasound in acetone and ethanol for 10 min, respectively. Then, the cleaned metal substances were soaked in 3 M HCl for 10 min to remove the oxide layer from the surface. 35.064 g NaCl (3 M) was added to 200 ml water to make a transparent corrosion solution in a galvanic cell (300 ml). And then, the cleaned NF and FF were immersed in the as-prepared solution by electrode holders. The two electrode holders were connected by wire to constitute a galvanic cell device. This galvanic corrosion process lasted for 48 hours under agitation. After the galvanic corrosion process, the NF was washed with ethanol and water several times. The electrode is labeled as GC NiFe LDH/Cl. The working area of the electrode is 1 cm^2. The loadings of the catalysts present at the NF surface are 2.1 mg cm^{-2}, which are calculated by the mass before and after the GC reaction.

In addition, several other halogen anions (NaF, NaBr, and NaI) were also used to replace Cl⁻ anions to prepare the corrosive solutions, which were labeled as GC NiFe LDH/F, GC NiFe LDH/Br and GC NiFe LDH/I.

1.2.2 Characterizations

XRD was carried out on Bruker AXS, D8 Advance X-ray powder diffractometer with Cu-K α radiation (λ = 0.15418 nm). Field-emission scanning electron microscope (FESEM) was performed on the Hitachi S-4800. TEM and HRTEM were obtained in the JEM-F200 transmission electron microscope. Raman spectra were carried out on LabRAM HR Evolution. The X-ray photoelectron spectroscopy (XPS) was performed on a Thermo Scientific ESCALAB 250Xi system.

1.2.3 Electrochemical Measurements

All electrochemical measurements were performed on an electrochemical workstation (CHI 760E, CH Instruments Inc., Shanghai). Hg/HgO electrode was used as the reference electrode and a carbon rod as the counter electrode. OER performances were measured by performing LSV (scan rate of 5 mV s⁻¹) in 1.0 M KOH solution with O₂-saturationand all initial data were corrected against the ohmic potential drop with 90% iR correction unless otherwise noted. All the potentials reported for OER were converted to the potential versus RHE according to E versus RHE = E Hg/HgO + 0.098 + 0.059 pH. EIS test was carried out in the range of 100 kHz to 0.1 Hz at a potential of 1.55 V vs. RHE with an AC amplitude of 10 mV. The long-time stability was quantified by recording a chronopotentiometry technique for three-electrode and two-electrode systems. The ESCA was tested with the scan rate of 50, 60, 70, 80, 90, and 100 at mV/s a potential ranging from 0.8-0.9 V vs. RHE. By plotting the difference of current density (J) between the anodic and cathodic sweeps ($J_{anodic} - J_{cathodic}$) at 0.85 V vs. RHE against the scan rate, a linear trend was observed. The slope of the fitting line is equal to twice the geometric double layer capacitance (C_{dl}), which is proportional to the effective electrode surface area of the materials. Therefore, we can compare the electrochemical surface areas of different samples based on their C_{dl} values.
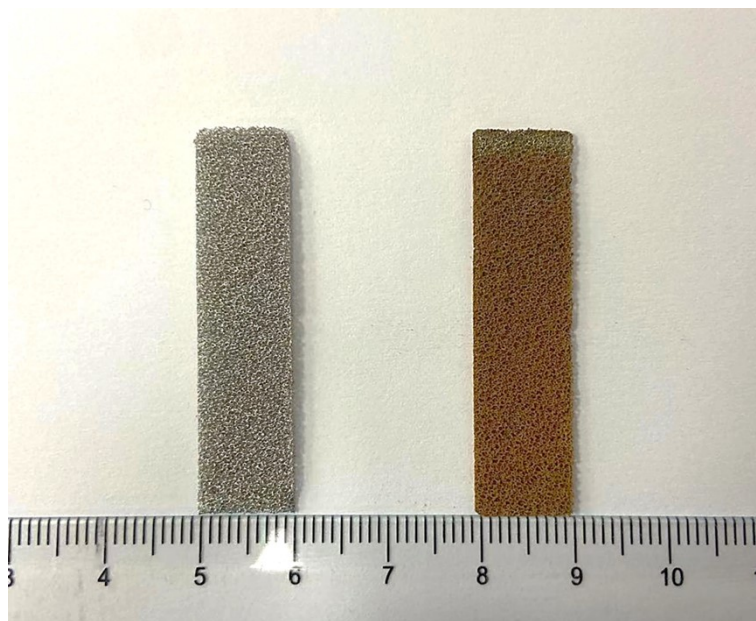
Supplementary Figures

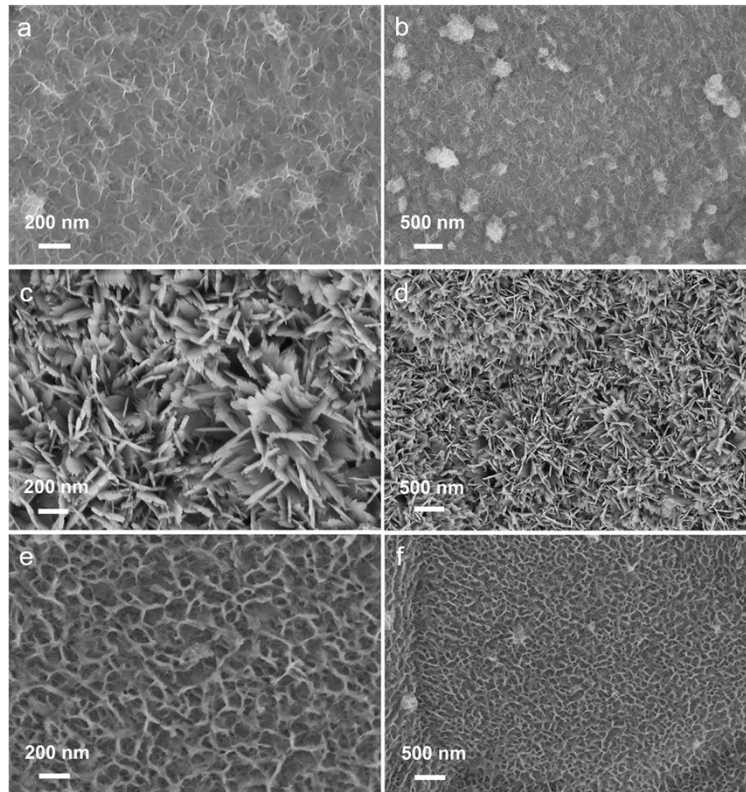Fig. S1 Photo of the bare NF (left) and GC NiFe LDH/Cl (right).

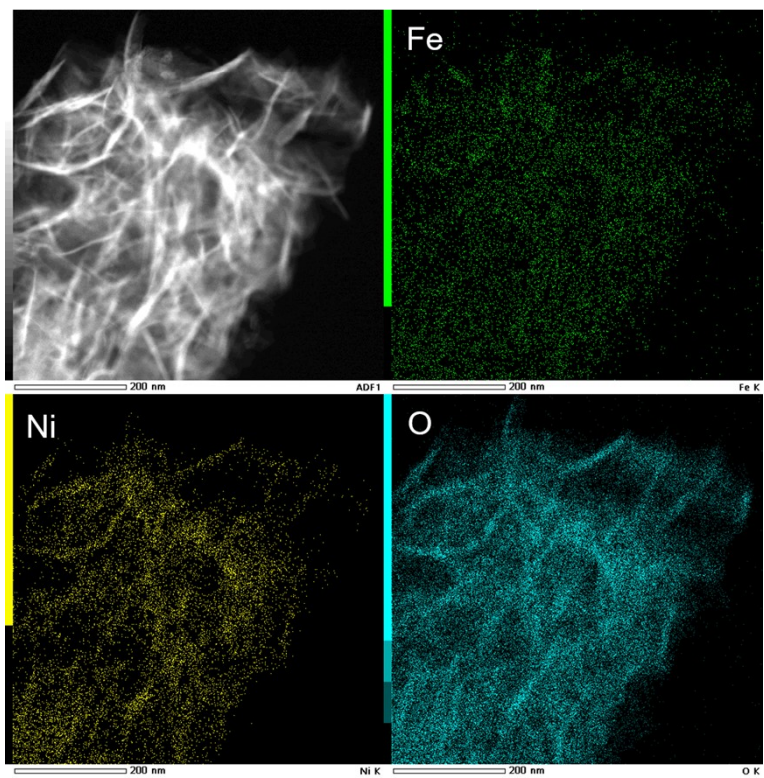Fig. S2 SEM images of (a, b) GC NiFe LDH/F, (c, d) GC NiFe LDH/Br, and (e, f) GC NiFe LDH/I.

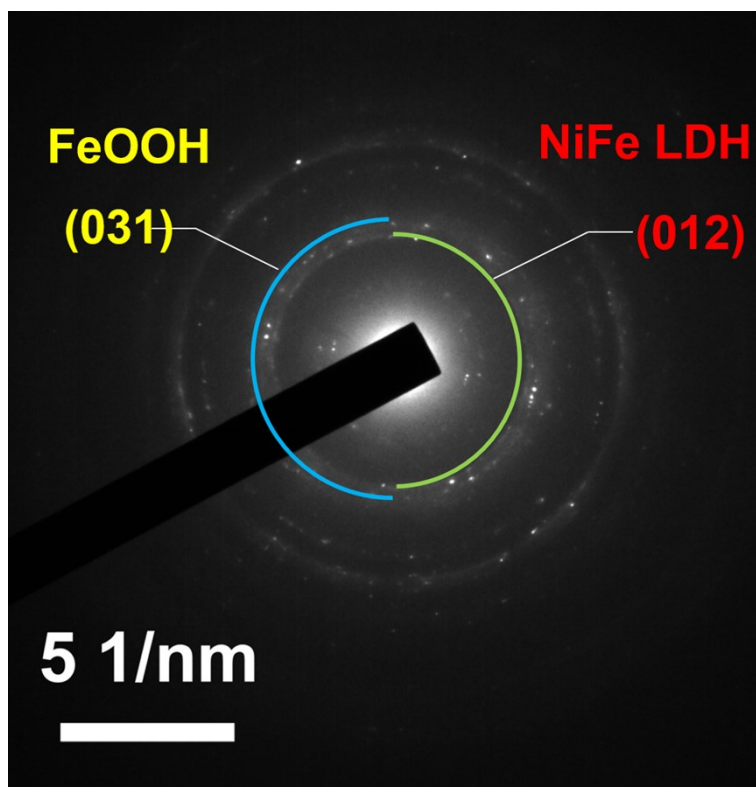Fig. S3 EDS mapping analysis of NiFe LDH/Cl

Fig. S4 SAED pattern of GC NiFe LDH/Cl.

Tab. S1 Elemental composition of as-prepared samples by ICP.

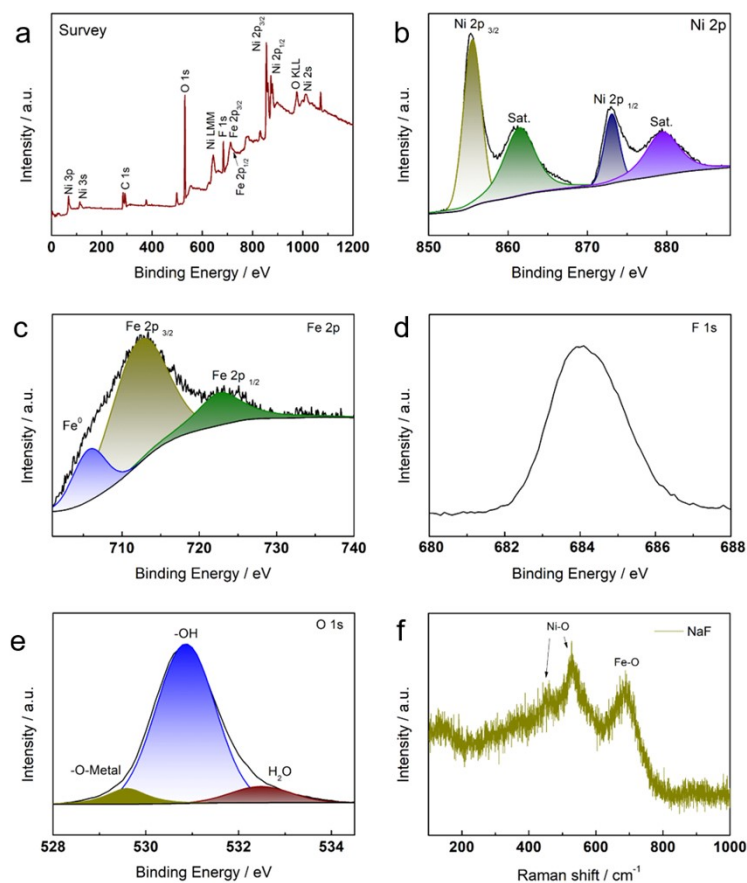| Sample	Ni wt%	Fe wt%
GC NiFe LDH/Cl	93.44	6.56
GC NiFe LDH/F	98.25	1.75
GC NiFe LDH/Br	92	8
GC NiFe LDH/I	90.6	9.4

Fig. S5 High-resolution XPS spectra in the regions of a) survey spectra, b) Ni 2p, c) Fe 2p, d) Cl 2p, and e) O1s, Raman spectra f) for GC NiFe LDH/F.

As depicted in Fig. S5, the survey spectra confirms that the GC NiFe LDH/F is composed of Fe, Ni, F, and O. In the Ni 2p high-resolution spectrum of GC NiFe LDH/F (Fig. S5b), the peaks at 855.5 and 873 eV correspond to the Ni^{2+}, accompanied by two prominent shakeup satellite peaks (861.6 and 879.6 eV)[1, 2]. Fig. S5c shows the core-level Fe 2p region spectrum and three peaks at 705.8, 712.8 and 725.4 eV correspond to the Fe^0, $2p_{3/2}$, and Fe $2p_{1/2}$, respectively, indicating the presence of Fe (III)[3]. Moreover, the peak at 684.1 eV in the F 1s spectrum (Fig. S5d) is assigned to Ni−F feature bonds[4]. About the high-resolution spectrum for O 1s (Fig. S5e), there are three peaks located at 528.8, 530.9, and 533 eV that can be attributed to the metal-O, hydroxyl groups and water molecules adsorbed on the surface, respectively[5]. The Raman spectra of GC NiFe LDH/F is the same as GC NiFe LDH/Cl, which also shows the characteristic peak of NiFe LDH.
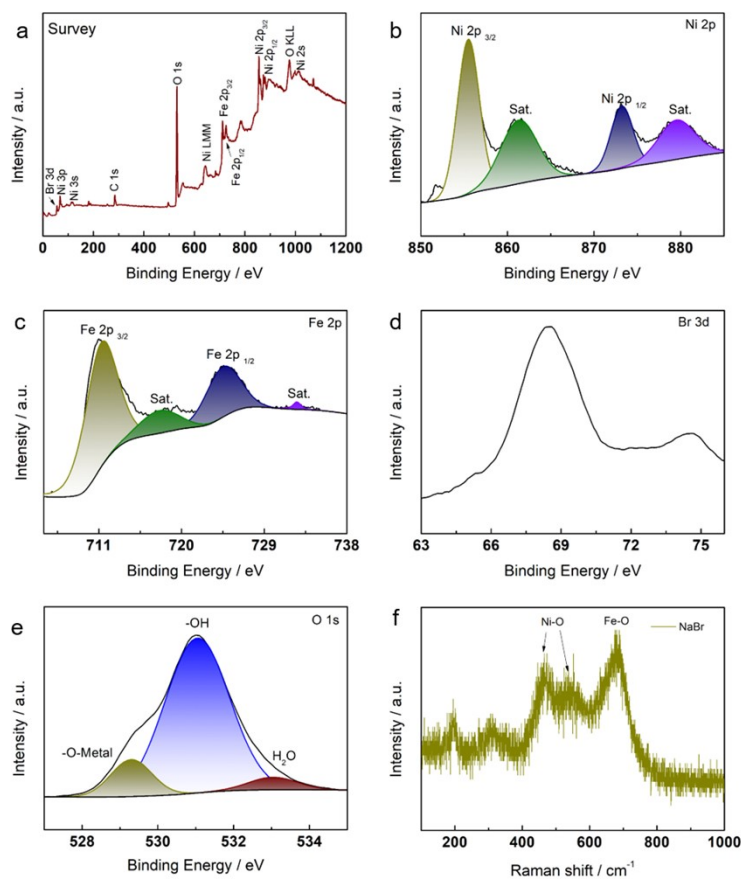
Fig. S6 High-resolution XPS spectra in the regions of a) survey spectra, b) Ni 2p, c) Fe 2p, d) Cl 2p, and e) O1s, Raman spectra f) for GC NiFe LDH/Br.

As shown in Fig. S6, the survey spectra confirm that the GC NiFe LDH/Br is composed of Fe, Ni, Br, and O. The Ni 2p high-resolution spectrum of GC NiFe LDH/Br (Fig. S6b) is the same as GC NiFe LDH/F (Fig. S5b). The high-resolution Fe 2p region in Fig. S6c exhibits four binding peaks at 711.4, 725, 717.5 and 732.6 eV belong to Fe $2p_{3/2}$, Fe $2p_{1/2}$ and two satellite peaks, suggesting the +3 oxidation state of the Fe species in GC NiFe LDH/Br. Moreover, the peak at 68.5 eV in Fig. S6d is assigned to Br 4d feature bonds[6]. About the high-resolution spectrum for O 1s (Fig. S6e, there are three peaks located at 528.8, 530.9, and 533 eV that can be attributed to the metal-O, hydroxyl groups, and water molecules adsorbed on the surface, respectively. The Raman spectra of GC NiFe LDH/Br (Fig. S6f) is the same as GC NiFe LDH/Cl, which also shows the characteristic peaks of NiFe LDH.
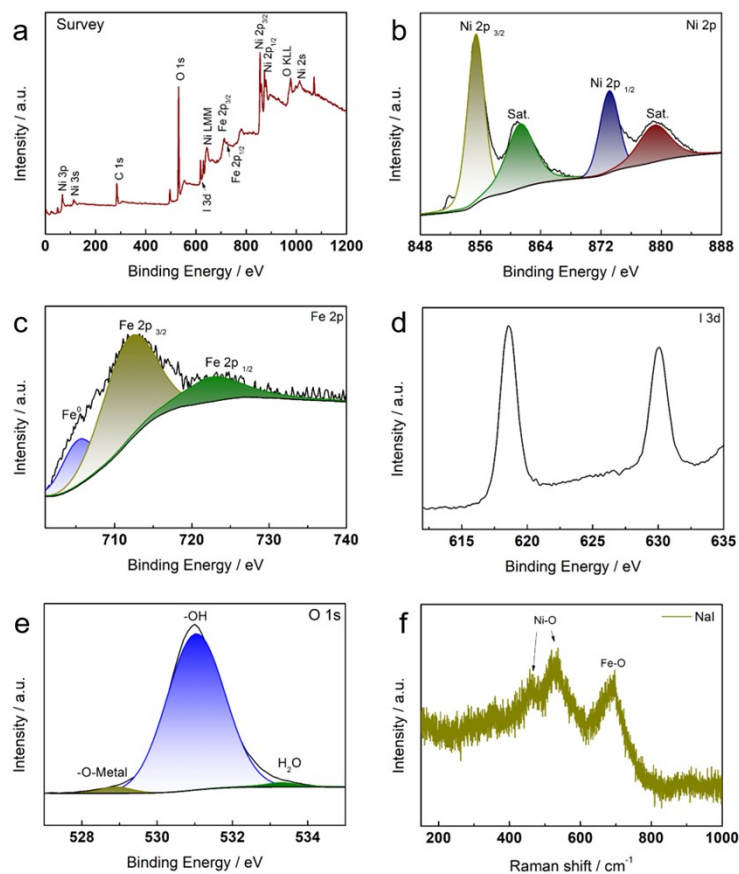
Fig. S7 High-resolution XPS spectra in the regions of a) survey spectra, b) Ni 2p, c) Fe 2p, d) Cl 2p, and e) O1s, Raman spectra f) for GC NiFe LDH/I.

As shown in Fig. S7, the survey spectra confirm that the GC NiFe LDH/I are composed of Fe, Ni, Br, and O. The Ni 2p, Fe 2p, and O1s high-resolution spectrum of GC NiFe LDH/I (Fig. S7b, c, and e) is the same as GC NiFe LDH/F. Moreover, the peaks at 618.5 and 630.1 eV in Fig. S7d) are assigned to I 3d feature bonds[6]. The Raman spectra of GC NiFe LDH/I is shown in Fig. S7f, it also shows the three characteristic peaks of NiFe LDH.
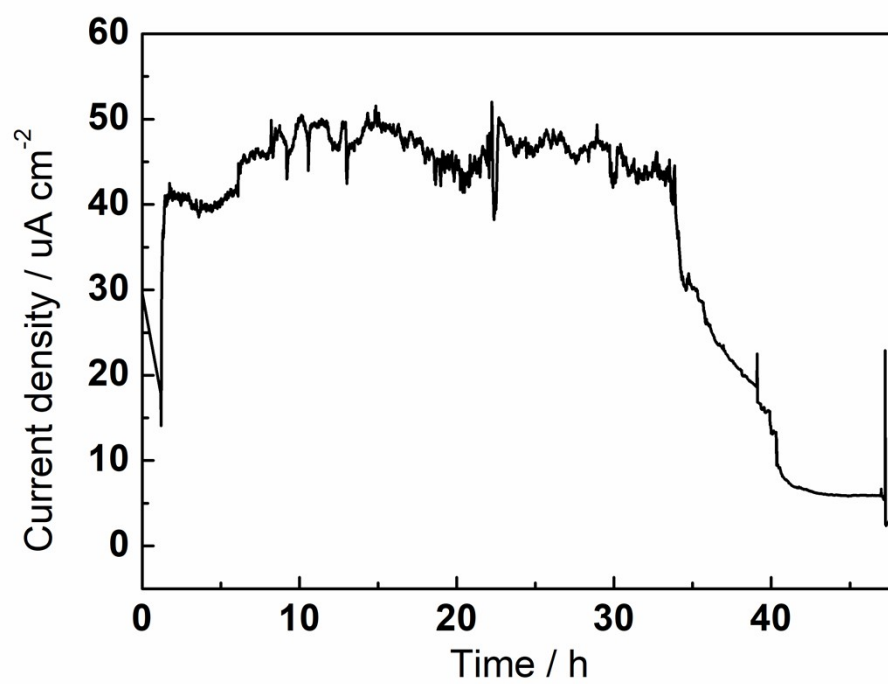
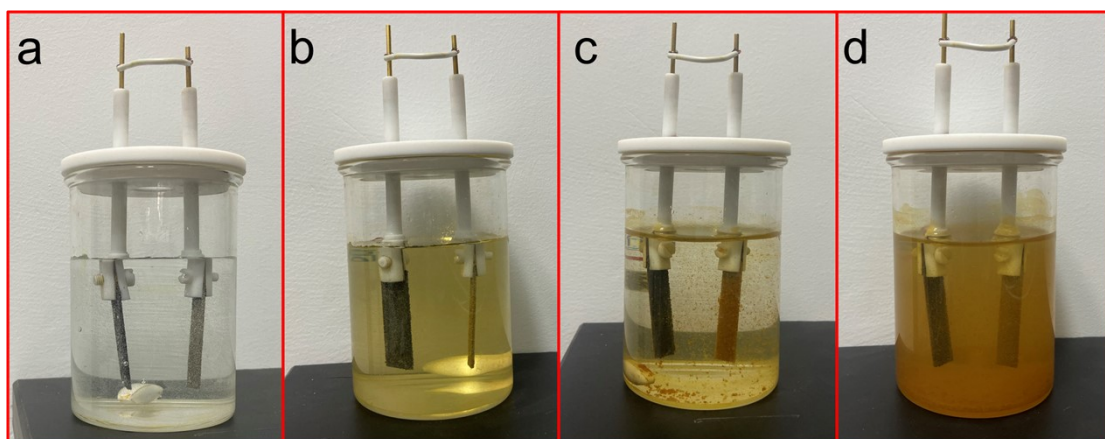Fig. S8 I-t curve of galvanic-cell corrosion process.

Fig. S9 The reaction time diagram of galvanic-cell corrosion. a) 0 h, b) 1 h, c) 6 h and d) 48 h.
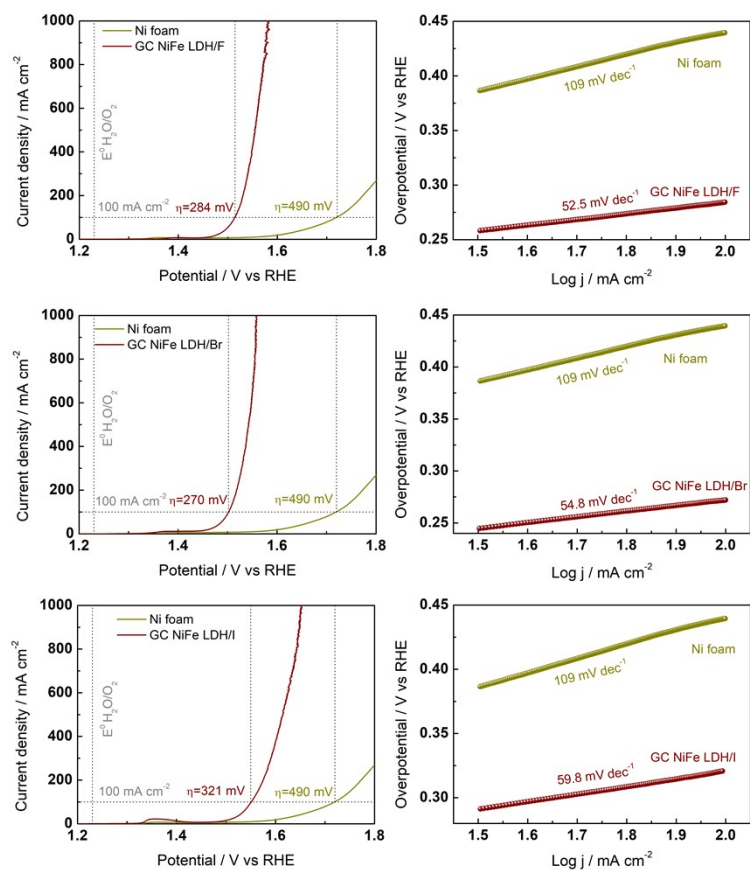
Fig. S10 LSV curves and corresponding Tafel plots of (a, b) GC NiFe LDH/F, (c, d) GC NiFe LDH/Br, and (e, f) GC NiFe LDH/I.
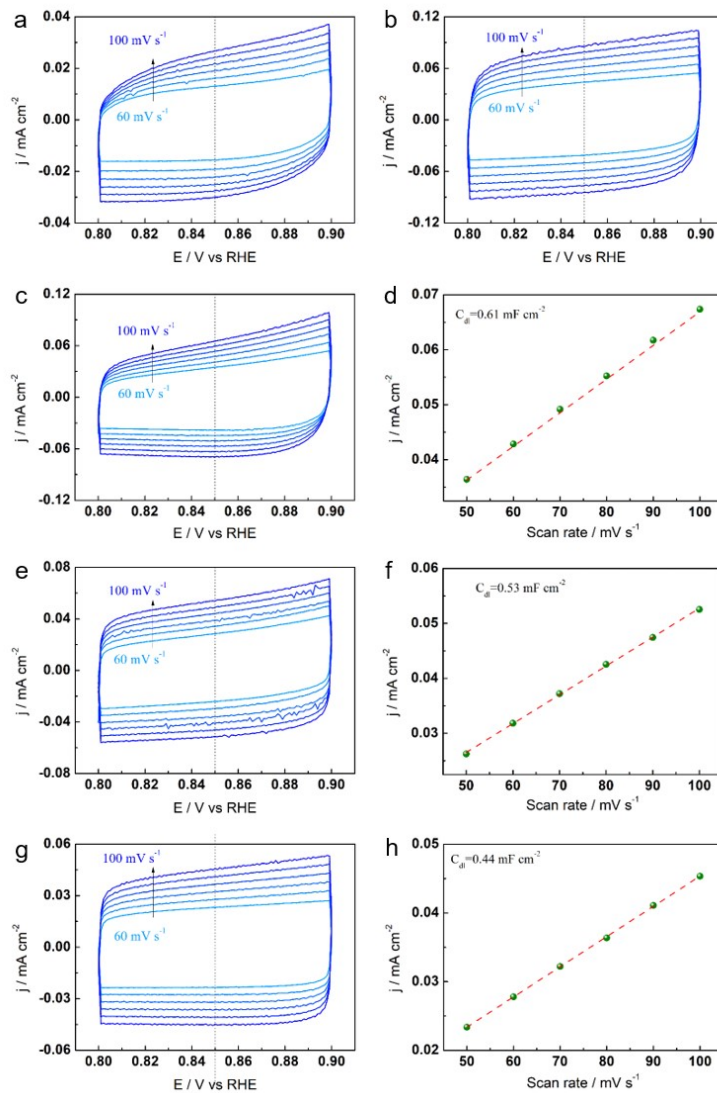
Fig. S11 Cyclic voltammograms curves of a) bare Ni foam, b) GC NiFe LDH/Cl, c) GC NiFe LDH/F, e) GC NiFe LDH/Br, and g) GC NiFe LDH/I. Charge current density differences (ΔJ) plotted against scan rate of d) GC NiFe LDH/F, f) GC NiFe LDH/Br, and h) GC NiFe LDH/I.
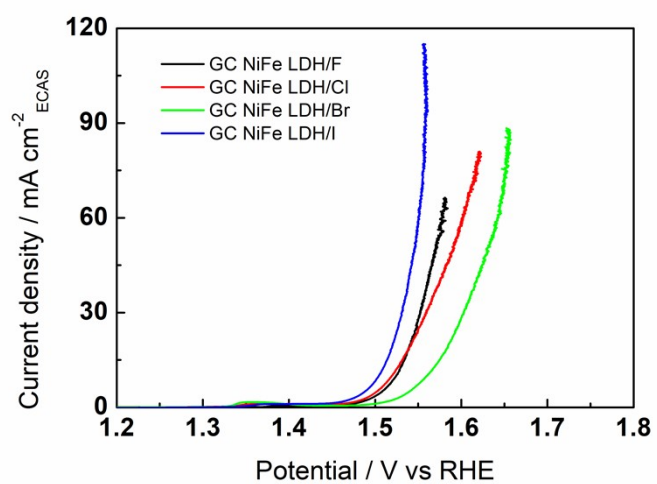
Fig.12 ECSA-normalized OER polarization curves of GC NiFe LDH.

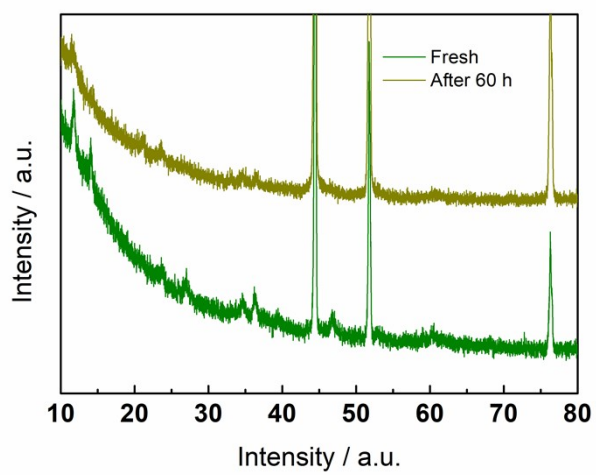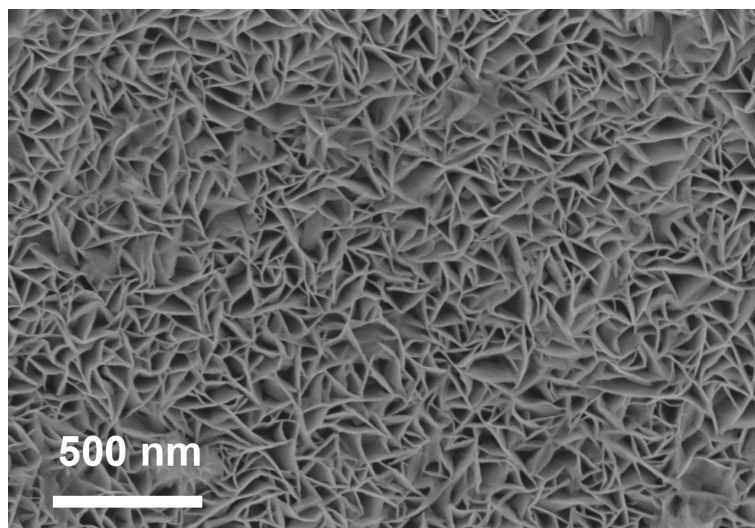Fig. S13 XRD patterns of fresh GC NiFe LDH/Cl and after 60 h chronopotentiometry test.

Fig. S14 SEM image of GC NiFe LDH/Cl after 60 h chronopotentiometry test.
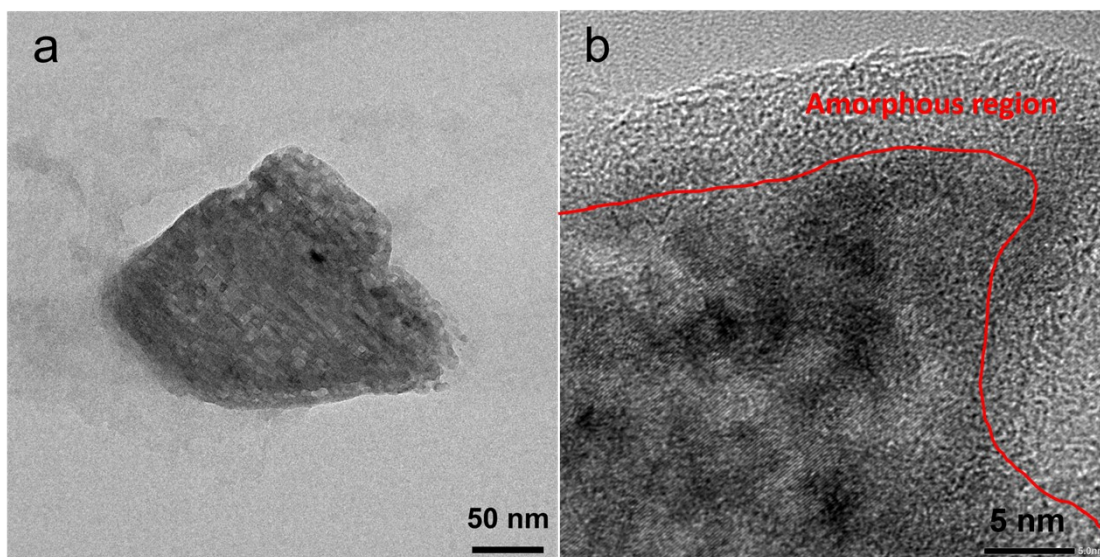
Fig. S15 a) TEM and b) HRTEM images of GC NiFe LDH/Cl after 60 h chronopotentiometry test.
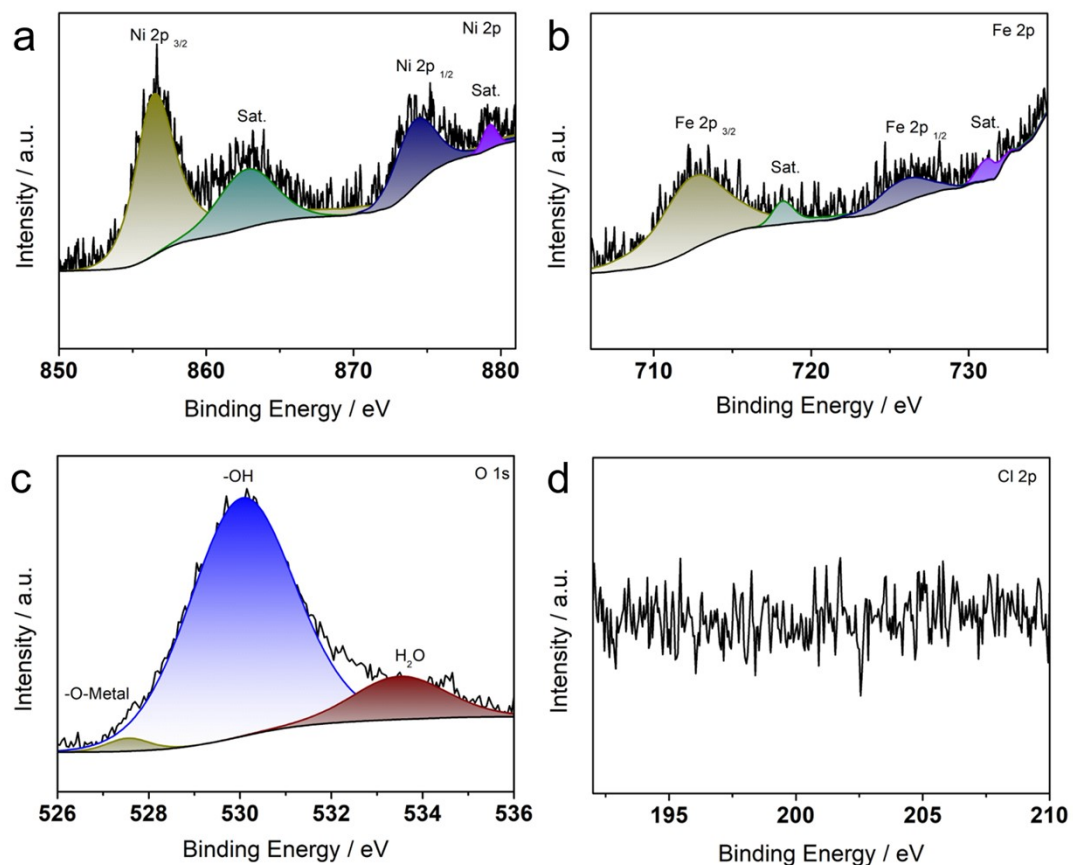
Fig. S16 High-resolution XPS spectra in the regions of a) Ni 2p, b) Fe 2p, c) O1s, and d) Cl 2p for GC NiFe LDH/Cl after 60 h chronopotentiometry test.

Tab. S2 OER performances of GC NiFe LDH/Br and other reported electrocatalysts

catalyst	Electrolyte	J/mAcm^{-2}	η/mV	Ref
GC NiFe LDH/Br	1 M KOH	100	270	This work
Ni$_{1.5}$Sn@triMPO$_4$	1 M KOH	100	330	[7]
δ -FeOOH NSs/NF	1 M KOH	100	~320	[8]
sd-NFF	1 M KOH	100	310	[9]
Ta-NiFe LDH	1 M KOH	100	280	[10]
NiMoFeO@NC	1 M KOH	100	290	[11]
Ni$_{0.83}$Fe$_{0.17}$(OH)$_2$	1 M KOH	100	350	[12]
S-(Ni,Fe)OOH	1 M KOH	100	281	[13]
Ni(Fe)OOH–FeS$_x$	1 M KOH	100	310	[14]
FeCoNiOOH	1 M KOH	100	330	[15]
NiFeO$_x$/NiFeOOH	1 M KOH	100	280	[16]
γ-FeOOH/NF	1 M KOH	100	320	[17]
FeNi@FeNiB-700	1 M KOH	100	399	[18]
NiFe/NiCo$_2$O$_4$	1 M KOH	100	~290	[19]
Cu@NiFe LDH	1 M KOH	100	281	[20]
NiFe/Ni(OH)$_2$/NiAl	1 M KOH	100	~400	[21]
Ni-Fe LDH	1 M KOH	10	280	[22]
N-SN	1 M KOH	100	365	[23]
MoFe:Ni(OH)$_2$/NiOOH	1 M KOH	100	~300	[24]
Fe-Ni$_3$S$_2$	1 M KOH	100	290	[25]
NiFeCr-6:2:1	1 M KOH	10	280	[26]
NiO/NiFe$_2$O$_4$	1 M KOH	10	279	[27]

1. Q. Liu, L. Xie, Z. Liu, G. Du, A. M. Asiri and X. Sun, *Chem. Commun.*, 2017, **53**, 12446-12449.

2. L. Wang, Y. Li, Q. Sun, Q. Qiang, Y. Shen, Y. Ma, Z. Wang and C. Zhao, *ChemCatChem*, 2019, **11**, 2011-2016.

3. Z. W. Gao, J. Y. Liu, X. M. Chen, X. L. Zheng, J. Mao, H. Liu, T. Ma, L. Li, W. C. Wang and X. W. Du, *Adv. Mater.*, 2019, **31**, e1804769.

4. W. He, L. Han, Q. Hao, X. Zheng, Y. Li, J. Zhang, C. Liu, H. Liu and H. L. Xin, *ACS Energy Lett.*, 2019, **4**, 2905-2912.

5. L. W. Jiang, Y. Huang, Y. Zou, C. Meng, Y. Xiao, H. Liu and J. J. Wang, *Adv. Energy Mater.*, 2022, **12**, 2202351.

6. H. Xu, J. Yan, Y. Xu, Y. Song, H. Li, J. Xia, C. Huang and H. Wan, *Appl. Catal., B*, 2013, **129**, 182-193.

7. S. Li, Z. Li, R. Ma, C. Gao, L. Liu, L. Hu, J. Zhu, T. Sun, Y. Tang, D. Liu and J. Wang, *Angew. Chem., Int. Ed.*, 2021, **60**, 3773-3780.

8. B. Liu, Y. Wang, H. Q. Peng, R. Yang, Z. Jiang, X. Zhou, C. S. Lee, H. Zhao and W. Zhang, *Adv. Mater.*, 2018, **30**, e1803144.

9. D. Li, Z. Pan, H. Tao, J. Li, W. Gu, B. Li, C. Zhong, Q. Jiang, C. Ye and Q. Zhou, *Chem. Commun.*, 2020, **56**, 12399-12402.

10. X. Wang, Y. Tuo, Y. Zhou, D. Wang, S. Wang and J. Zhang, *Chem. Eng. J.*, 2021, **403**, 126297.

11. Y. Wang, Y. Zhu, S. Zhao, S. She, F. Zhang, Y. Chen, T. Williams, T. Gengenbach, L. Zu, H. Mao, W. Zhou, Z. Shao, H. Wang, J. Tang, D. Zhao and C. Selomulya, *Matter*, 2020, **3**, 2124-2137.

12. Q. Zhou, Y. Chen, G. Zhao, Y. Lin, Z. Yu, X. Xu, X. Wang, H. K. Liu, W. Sun and S. X. Dou, *ACS Catal.*, 2018, **8**, 5382-5390.

13. L. Yu, L. Wu, B. McElhenny, S. Song, D. Luo, F. Zhang, Y. Yu, S. Chen and Z. Ren, *Energy Environ. Sci.*, 2020, **13**, 3439-3446.

14. H. Yang, L. Gong, H. Wang, C. Dong, J. Wang, K. Qi, H. Liu, X. Guo and B. Y. Xia, *Nat. Commun.*, 2020, **11**, 5075.

15. Q. Zhang, N. M. Bedford, J. Pan, X. Lu and R. Amal, *Adv. Energy Mater.*, 2019, **9**, 1901312.

16. H. Xu, J. Wei, K. Zhang, Y. Shiraishi and Y. Du, *ACS Appl. Mater. Interfaces*, 2018, **10**, 29647-29655.

17. K. Wang, H. Du, S. He, L. Liu, K. Yang, J. Sun, Y. Liu, Z. Du, L. Xie, W. Ai and W. Huang, *Adv. Mater.*, 2021, **33**, e2005587.

18. H. Yuan, S. Wang, X. Gu, B. Tang, J. Li and X. Wang, *J. Mater. Chem. A*, 2019, **7**, 19554-19564.

19. C. Xiao, Y. Li, X. Lu and C. Zhao, *Adv. Funct. Mater.*, 2016, **26**, 3515-3523.

20. L. Yu, H. Zhou, J. Sun, F. Qin, F. Yu, J. Bao, Y. Yu, S. Chen and Z. Ren, *Energy Environ. Sci.*, 2017, **10**, 1820-1827.

21. S. Niu, W. J. Jiang, T. Tang, Y. Zhang, J. H. Li and J. S. Hu, *Adv. Sci.*, 2017, **4**, 1700084.

22. L. Yu, J. F. Yang, B. Y. Guan, Y. Lu and X. W. D. Lou, *Angew. Chem., Int. Ed.*, 2018, **57**, 172-176.

23. K. Zhang, X. Xia, S. Deng, Y. Zhong, D. Xie, G. Pan, J. Wu, Q. Liu, X. Wang and J. Tu, *Nano-Micro Lett.*, 2019, **11**, 21.

24. Y. Jin, S. Huang, X. Yue, H. Du and P. K. Shen, *ACS Catal.*, 2018, **8**, 2359-2363.

25. D. Li, W. Wan, Z. Wang, H. Wu, S. Wu, T. Jiang, G. Cai, C. Jiang and F. Ren, *Adv. Energy Mater.*, 2022, **12**, 2201913.

26. Y. Yang, L. Dang, M. J. Shearer, H. Sheng, W. Li, J. Chen, P. Xiao, Y. Zhang, R. J. Hamers and S. Jin, *Adv. Energy Mater.*, 2018, **8**, 1703189.

27.   H. Zhong, G. Gao, X. Wang, H. Wu, S. Shen, W. Zuo, G. Cai, G. Wei, Y. Shi, D. Fu, C. Jiang, L. W. Wang and F. Ren, *Small*, 2021, **17**, e2103501.